DETECTION OF OFF-PULSE EMISSION FROM PSR B0525+21 AND PSR B2045−16

Rahul Basu[1], Ramana Athreya[2,3], and Dipanjan Mitra[1,4]

[1] National Centre for Radio Astrophysics, P.O. Bag 3, Pune University Campus, Pune, 411 007, India; rbasu@ncra.tifr.res.in, dmitra@ncra.tifr.res.in
[2] Indian Institute of Science Education Research (IISER)-Pune, 900, NCL Innovation Park, Homi Bhabha Road, Pune, 411 008, India; rathreya@iiserpune.ac.in

ABSTRACT

We report the detection of off-pulse emission from two long-period pulsars PSR B0525+21 and PSR B2045−16 using the Giant Metrewave Radio Telescope. We recorded high time resolution interferometric data at 325 MHz and gated the data off-line to separate the on- and off-pulse sections of the pulsar. On imaging the two temporal sections separately, we detected a point source in the off-pulse images of both the pulsars coincident with the pulsar locations in the on-pulse images. The long periods (3.75 and 1.96 s, respectively) and low spin-down energies ($\dot{E} \sim 10^{31}$ erg s^{-1}) of the two pulsars argue against a pulsar wind nebula (PWN) origin for the off-pulse emission. The derived estimates of the interstellar medium particle density required to drive a PWN do not support such an interpretation. A magnetospheric origin for the off-pulse emission raises questions regarding the location of the emission region, which is an important input into pulsar emission models.

Key words: pulsars: general – pulsars: individual (PSR B0525+21, PSR B2045−16)

Online-only material: color figure

1. INTRODUCTION

We report the detection of off-pulse emission from two long-period pulsars, PSR B0525+21 and PSR B2045−16, using the interferometric mode of the Giant Metrewave Radio Telescope (GMRT) in the 325 MHz frequency band. The "main-pulse" (or the equivalent term "on-pulse" used in this paper) is the emission from within the polar-cap region of a pulsar; and the off-pulse is the emission outside this main-pulse. Off-pulse emission from pulsars has been a subject of interest since the discovery of pulsars four decades ago.

According to the rotating vector model (RVM) proposed by Radhakrishnan & Cooke (1969) the observed pulses are due to relativistically beamed radiation along the open dipolar field lines. The plane of linear polarization traces the magnetic field line associated with the emission at every instant. Several statistical studies have revealed that pulsar radio emission is in the form of a circular beam arising from the polar cap (i.e., the main-pulse) with an opening angle ρ, and from a height above the magnetic pole equal to 1%–2% of the radius of the light cylinder. The width of the observed pulse is a geometrical function of ρ (which itself is a function of the emission height), the pulsar period, the angle between the rotation axis and the magnetic axis (α), and the angle between the magnetic axis and the line of sight to the observer (β). The angles α and β can be estimated by fitting the RVM to the swing of the polarization position angle (PPA) across the pulse (Everett & Weisberg 2001; Mitra & Li 2004).

The observed main-pulse covers 5%–10% of the pulsar period for 90% of the pulsars. In several pulsars this main-pulse consists of multiple components including low-level bridge emission between such components (Rathnasree & Rankin 1995). The pulse width scales as $1/\sin(\alpha)$, from the geometry of the emission model; in the rare case of a pulsar with closely aligned magnetic and rotation axes (i.e., $\alpha \sim 0°$ or $180°$), the pulse width can be as high as 100%. Several pulsars have low level but detectable bridge emission between two widely spaced pulse components, making them candidates for an aligned rotator geometry. In rare cases when α is close to $90°$, emission from the opposite pole (i.e., the inter-pulse) may be observed at the $180°$ phase from the main-pulse. In all these instances, the observed emission is believed to lie within the polar cap (i.e., main-pulse) as described earlier.

In a few pulsars, low-level emission components known as pre-/post-cursors (PPCs) have been observed outside the main-pulse (e.g., see Mitra & Rankin 2011 for a discussion). In these pulsars, all geometrical evidence indicate that the main-pulse is consistent with emission from open field lines. The PPC components appear highly polarized and are far from the main-pulse. The discovery of the PPC component about $60°$ away from the main-pulse in PSR B0943+10 is particularly interesting, as the line of sight almost grazes the emission cone for this pulsar (Backus et al. 2010). Hence, the PPC emission originates either from a much larger height, where due to spreading of dipolar field lines the PPC component can lie far away from the main-pulse, or from the regions of closed field lines. Some pulsars occasionally emit giant pulses which are believed to arise close to the light cylinder rather than the polar cap. Interestingly, PPC pulsars have low spin-down luminosities ($\dot{E} < 10^{34}$ erg s^{-1}), whereas the giant pulses arise from pulsars with $\dot{E} \gtrsim 10^{34}$ erg s^{-1}. The PPC components and giant pulses may be examples of magnetospheric off-pulse emission in pulsars. They challenge the conventional wisdom of pulsar radio emission arising only from open magnetic field lines close to the pulsar polar cap and raise questions about the origin of these emission components.

The other possible source of off-pulse emission is the interstellar medium (ISM) around the pulsar. The pulsar loses most of its rotational energy in the form of a relativistic wind which, when confined by the surroundings, may form a pulsar wind nebula (PWN). Several types of PWNe are formed depending on the confinement mechanism. Young and energetic pulsars are often located in their associated supernova remnant (SNR). The pulsar wind streaming into the ambient medium produces

---

[3] Author to whom any correspondence should be addressed.
[4] Part of the work was done while at NAIC, Arecibo Observatory, as a visiting scientist.

Table 1
Properties of Pulsars Selected for Off-pulse Studies

Pulsar	Period (s)	DM (cm^{-3} pc)	Dist. (kpc)	τ_c (year)	$\dot{E}$ (erg s^{-1})	$V_{\rm trans}$ (km s^{-1})	Flux$_{325}$ (mJy)
B0525+21	3.7455	50.937	2.28	1.48×10^6	3.0×10^{31}	229	80.5
B2045−16	1.9616	11.456	0.95	2.84×10^6	5.7×10^{31}	511	169.3

Notes. Period, dispersion measure, and proper motion (for $V_{\rm trans}$) are from Hobbs et al. (2004) and the others are from Taylor et al. (1993). Flux$_{325}$ is the expected flux at 325 MHz calculated from values in Lorimer et al. (1995).

standing shocks resulting in a plerionic PWN (like the one observed in the Crab nebula). In older pulsars, where the surrounding SNR is likely to be dissipated, the relativistic particles may interact with the ISM magnetic field and radiate, creating ghost remnants (proposed by Blandford et al. 1973, but not observed till date). Finally, a pulsar moving through the ISM with supersonic speed can produce a bow shock nebula, where ram pressure balance is established between the pulsar wind and the ambient medium. Several such bow shock nebulae have been detected in Hα, and some in the radio as plerionic bow shocks, but never in both (see Chatterjee & Cordes 2002 for a detailed study).

Several searches for PWNe have been conducted in the past with varying sensitivities and resolutions. However, only in about 10 young pulsars have radio emission been detected outside the main-pulse and all of these are believed to be associated with PWNe. In all such cases, the associated pulsars are young (10^3–10^5 yr), have high spin-down luminosities ($\dot{E} \gtrsim 10^{35}$ erg s^{-1}), and all except one are associated with SNRs (Gaensler et al. 1998; Gaensler et al. 2000; Stappers et al. 1999). It is believed that the pulsar wind and the environment change as pulsars slow down and age, making them less likely to harbor PWNe.

The present study was designed to detect radio emission away from the polar caps and not associated with PWNe. Therefore, we targeted old and less energetic pulsars unlikely to harbor PWNe. Their profiles did not show any components outside the main-pulse. The targets were neither aligned rotators nor inter-pulsars. We attempted to detect emission within a pulse longitudinal range of approximately $80°$–$250°$ from the peak in the main-pulse.

We describe the gated interferometric observations and the data analysis in Section 2, the results in Section 3, the additional tests we carried out to confirm that the off-pulse emission were not instrumental artifacts in Section 4, and discuss the implications of the detections in Section 5.

2. OBSERVATIONS AND ANALYSIS

2.1. Target Pulsars

We chose two pulsars, B0525+21 and B2045−16, whose pulse profiles did not show any features outside the main-pulse (Gould & Lyne 1998) and were stronger than 50 mJy to be able to put a non-detection upper limit of at most 5% of the pulsed flux. The properties of the targets are listed in Table 1. We targeted long-period pulsars because:

1. PWNe are so far only known from short-period, energetic pulsars in the vicinity of SNRs. A long period selects against both high energy pulsars and SNR association, and hence PWNe.
2. We wanted at least eight bins (of 131 or 262 ms each) across the pulse period to separate cleanly the off-pulse and the

on-pulse regions.

The temporal broadening across the 16 MHz bandwidth due to dispersion by the ISM was 183.3 ms for PSR B0525+21 (bin width 262 ms, gate width 1.31 s) and 47.8 ms for PSR B2045−16 (bin width 131 ms, gate width 0.655 s). Therefore, we did not have to dedisperse the signal.

2.2. Interferometric Imaging of the Pulsars with the GMRT

Interferometric observations are better than single-dish measurements for this study for several reasons.

1. An imaging interferometer is only insensitive to the constant flux-density background along the spatial axes while a standard pulsar receiver is usually insensitive to the constant background along the time axis; the detection of off-pulse emission is essentially an attempt to find such a constant background along the time axis.
2. Self-calibration of interferometric data can correct instrumental and atmospheric gain fluctuations on very short timescales. The corrections are determined by the flux densities of the constant and bright background sources in the field and hence would not be affected by the pulse variation of the relatively weak pulsar.
3. The higher spatial resolution of an interferometer greatly reduces the coincidence of unrelated sources, thereby reducing the probability that the off-pulse emission is from an unrelated source within the synthesized beam.

We imaged the pulsars with the GMRT, an aperture-synthesis radio interferometer located near Pune, India (Swarup et al. 1991). The 30 antennas of 45 m diameter provide a maximum baseline of 27 km and can be operated at 6 frequency bands between 50 and 1450 MHz. We observed the pulsars at 325 MHz with a 16 MHz bandwidth split into 128 channels. The frequency was chosen for its optimal combination of resolution ($10''$) and sensitivity (few 100 μJy in 4 hr of observing). The high-frequency resolution was useful in flagging narrow-band radio-frequency interference (RFI) and to avoid bandwidth smearing. The shortest integration output by the hardware correlator is 0.131 s, though these data are usually averaged and median filtered to provide a standard data output integration of 16.77 s.

The two pulsars were first observed on 2009 May 19 with 0.262 s integration to keep the data output rate and size manageable. This time resolution (of 7 bins) was found to be inadequate in the case of PSR B2045−16 while the data were of poor quality (> 10 missing antennas) for both targets. We re-observed the sources on 2010 January 19, with integrations of 0.131 s for PSR B2045−16 (period 1.9616 s) and 0.262 s for PSR B0525+21 (period 3.7455 s). This allowed us to divide both pulsar periods into 14 time bins.

2.3. Data Analysis

Several earlier studies used the technique of online gating to separate the on- and off-pulse regions using the timing
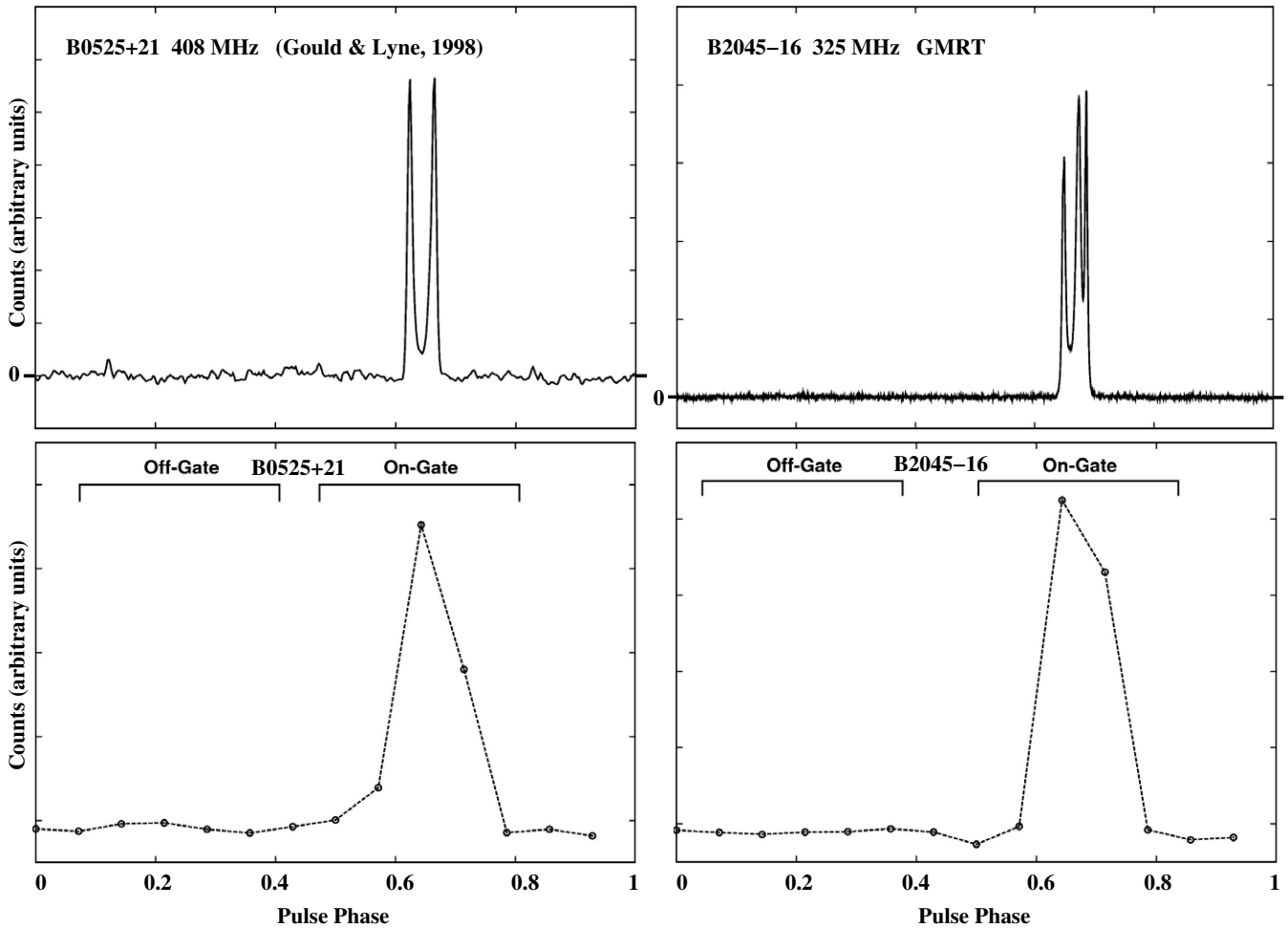
Figure 1. Pulse profiles for our targets from standard pulsar mode high time resolution observations (top row) and our folded interferometric self data at 325 MHz (bottom row).

information of pulsars and accumulated time-averaged on- and off-pulse data (Strom & Van Someren Greve 1990; Stappers et al. 1999). This resulted in relatively smaller size of data files and hence shorter computation times which was a major consideration one to two decades ago. The disadvantage was the impossibility of rectifying any errors during the gating process (see results and discussions in Gaensler et al. 2000). We recorded the data at sufficiently high resolution and applied off-line gating.

2.3.1. Folding and Gating

In the absence of accurate absolute time reference in the interferometric mode, we used off-line gating to isolate the off-pulse region of the pulsar period. The 30 antennas of GMRT provide 30 self and 435 cross visibilities at each integration interval (0.131 s or 0.262 s). We folded the self-data to obtain the pulsar profile and identify the on- and off-pulse regions. This was used to gate the cross-antenna visibilities into on- and off-pulse data sets.

The temporal and frequency gain variations in the self-data were corrected by normalizing the instantaneous values by the local median. The timescale for the temporal median was 30–50 times the pulsar period to ensure that the pulse variation was retained. The data from all frequency channels and antennas were averaged with robust sigma-clipping and processed using the standard folding algorithm for pulsars (Hankins & Rickett

1975) to determine the pulse profile. The pulsar profiles and the off- and on-pulse gates are shown in Figure 1.

The off- and on-pulse gates of PSR B0525+21 were centered on phases 0.24 and 0.64, respectively. The five bins nearest to each were averaged to construct the off- and on-pulse data sets. The corresponding phases for PSR B2045−16 were 0.21 and 0.67, respectively. The folding and gating procedures were carried out using software developed for this purpose.

2.3.2. Imaging

The on- and off-pulse data were cleaned of RFI using the RfiX algorithm (Athreya 2009). They were separately calibrated, flagged, and imaged in a standard manner using the NRAO AIPS package. The flux-density scale of the images was determined from observations of the calibrator 3C48 and the measurements of Baars et al. (1977) with the latest corrections of Perley et al. (1999; in AIPS). The data sets were taken through several rounds of phase self-calibration followed by a final round of amplitude and phase self-calibration.

PSR B0525+21. Observations of the calibrator 0521+166 were interspersed with the target to correct for the amplitude and phase gain fluctuations. The presence of the extremely strong and extended crab nebula (flux > 1000 Jy and angular size $\sim 10'$) at the edge of the primary beam ($1°5$ away) resulted in enhanced noise and strong ripples in the initial image. Therefore, subsequent analyses were carried out with a lower UV cutoff at
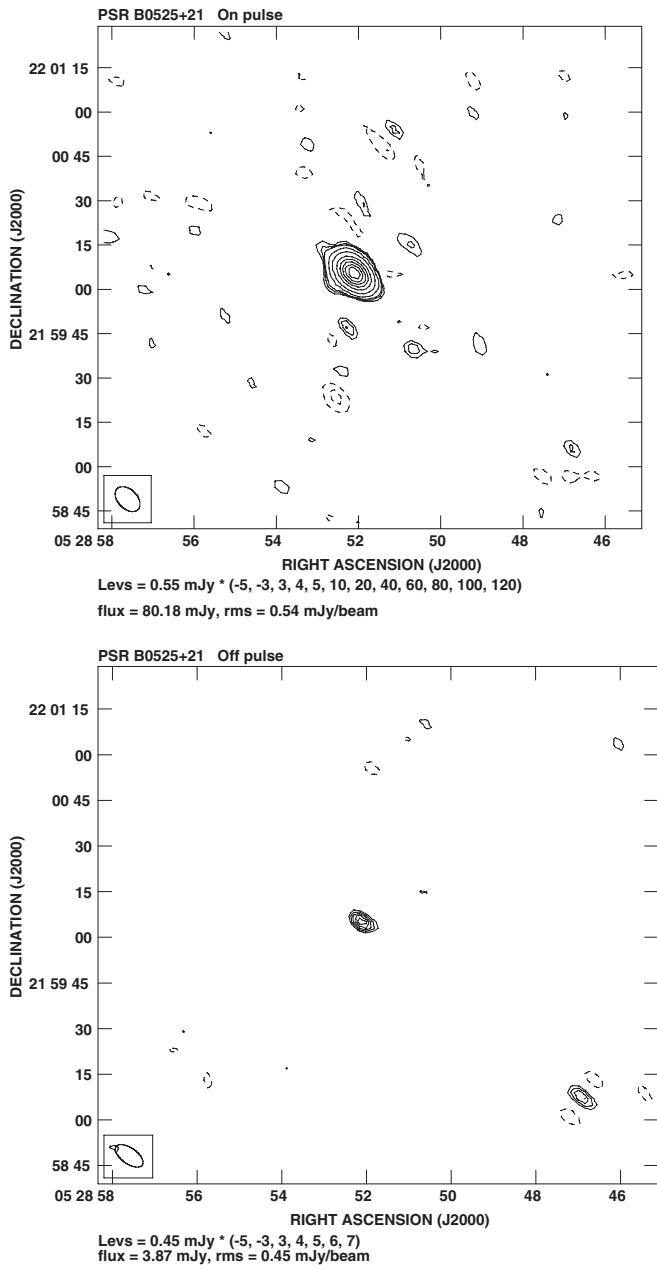
Figure 2. Contour plots of the on- and off-pulse images of B0525+21 showing the pulsar detection. The synthesized beam is shown in the box.

1.5 kλ which reduced the artifacts and noise. This eliminated all structures larger than 2′.3 from the image; this did not affect our purpose as our target source was expected to be much smaller than 2′.

PSR B2045–16. The calibrator 2137–207 was observed for amplitude and phase calibration. A pointing error resulted in the pulsar being located 35′ away from the field center (60% gain level of the primary beam). The primary beam correction was applied to the image to obtain the correct flux density for the pulsar.

3. RESULTS

We detected off-pulse emission in both the pulsars, coincident with the location in the on-pulse image (Figures 2 and 3). The results are summarized in Table 2. The on- and off-pulse emissions appeared to be unresolved for both pulsars.
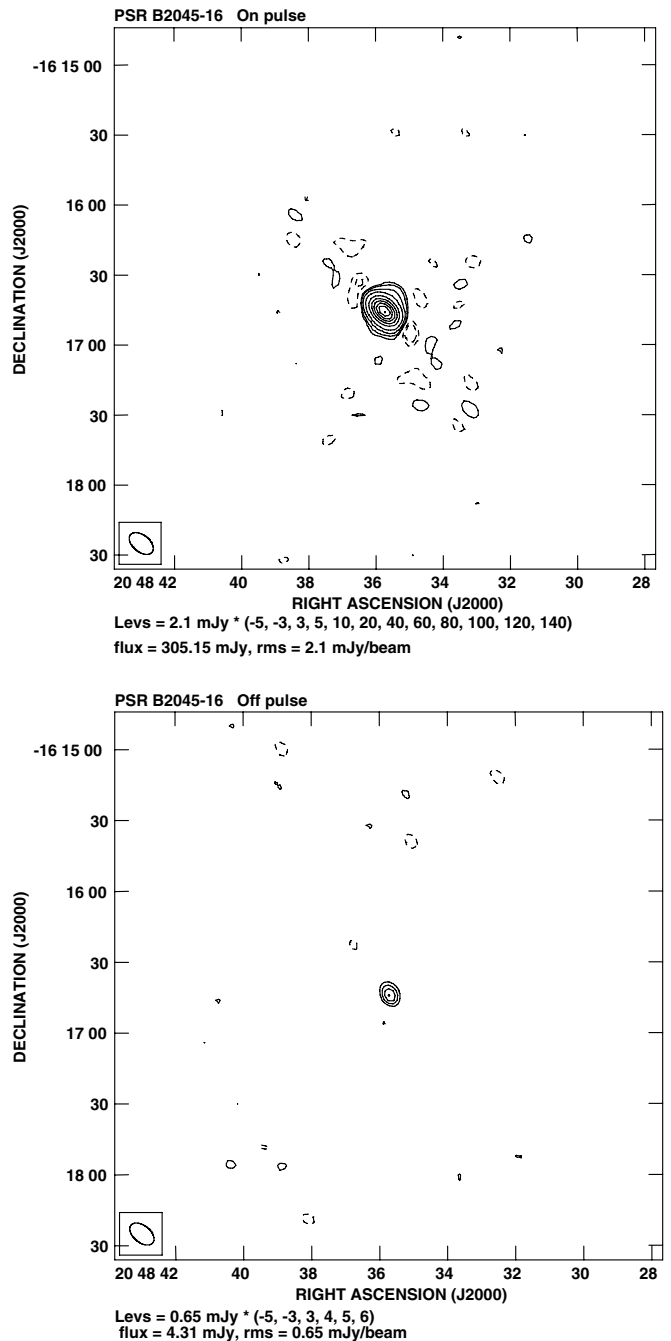

Figure 3. Contour plots of the on- and off-pulse images of B2045–16 showing the pulsar detection. The synthesized beam is shown in the box.

We compared the flux densities of sources in the field of view to check the flux-density calibration. The ratios of on- and off-image flux densities of sources stronger than 10 mJy are plotted in Figure 4. There were 43 and 93 comparison sources in the fields of B0525+21 and B2045–16, respectively. The scatter of values around unity, especially for strong sources (which have smaller fractional flux errors), confirmed the similarity of the flux scale of the on- and off-images for both the pulsars.

PSR B0525+21. The pulsar was detected in the off-pulse image at the 8.6σ level (flux density 3.9 ± 0.5 mJy, rms noise 0.45 mJy beam^{-1}). The flux density of the pulsar in the on-pulse image was 80.2 ± 5.8 mJy (rms noise 0.55 mJy beam^{-1}). The resolution element at the distance of the pulsar corresponds

Table 2
Summary of On- and Off-pulse Observations and Results

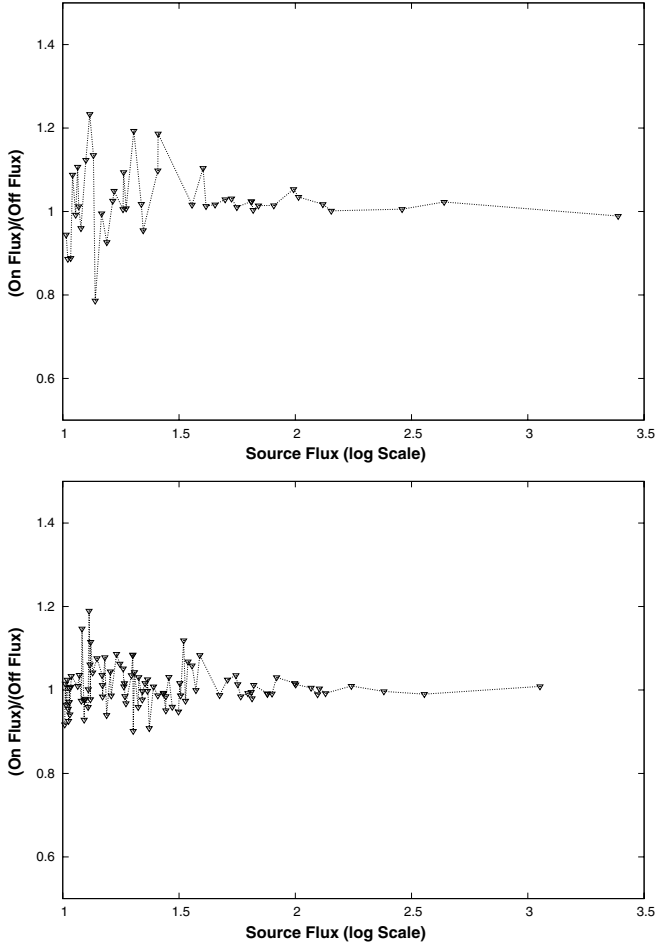| Pulsar	Frequency (MHz)	Time (min)	Beam ('')	Size (pc)	On rms (mJy beam^{-1})	On Flux (mJy beam^{-1})	Off rms (mJy beam^{-1})	Off Flux (mJy beam^{-1})	Avg. Flux (mJy beam^{-1})
B0525+21	332.9	160	9.5×6.5	0.088	0.55	80.2 ± 5.8	0.45	3.9 ± 0.5	30.0 ± 2.1
B2045−16	317.1	180	11.9×7.2	0.042	2.10	305 ± 22	0.65	4.3 ± 1.1	110.5 ± 7.9

Figure 4. Ratio of the measured flux densities of point sources (flux density > 10 mJy) in the on- and off-pulse images. The scatter around unity confirmed that the flux scale was the same for both. (B0525+21: top; B2045−16: bottom).

to 0.09 pc. The data from 2009 May 19 yielded an off-pulse detection of 3.6 mJy.

PSR B2045−16. The pulsar was detected in the off-pulse image at the 6.6σ level (flux density 4.3 ± 1.1 mJy; rms noise 0.65 mJy beam^{-1}). The flux density of the pulsar in the on-pulse image was 305.2 ± 21.9 mJy (rms noise 2.1 mJy beam^{-1}). The resolution element at the distance of the pulsar corresponds to 0.04 pc.

The flux densities averaged over the entire pulsar period is 30.0 ± 2.1 for B0525+21 and 110.5 ± 7.9 for B2045−16. These values are smaller than expected (Table 1) by factors of 2.7 and 1.5, which can be caused by effects such as refractive interstellar scintillations (Stinebring & Condon 1990). We confirmed the correctness of our flux scale by comparing the flux densities of the phase calibrators to their known values (less than 1%) and by comparing the flux densities of three to five strong sources in each field to the interpolated values from NVSS (1.4 GHz) and VLSS (74 MHz).

The quoted errors on the flux densities were obtained by adding in quadrature the image rms, calibration errors, and the error on the value of the primary flux-density calibrator (Baars et al. 1977).

The signal-to-noise ratio in the published profiles of the pulsars (Gould & Lyne 1998) is insufficient to conclude whether the off-pulse emission detected here is a pedestal (throughout the period) or a pulse confined to the off-pulse gate.

4. GENUINENESS OF THE OFF-PULSE DETECTION

First, we detected the off-pulse emission in two data sets of B0525+21 observed eight months apart and within the noise the two measurements were identical. We can safely rule out the detections being chance occurrence of noise peaks. Second, B2045−16 was positioned almost at the half-power point of the primary beam while B0525+21 was close to the field center. The detection in both cases suggests that they are not the spurious structures occasionally seen at the center of the field. We discuss below several effects which could result in spurious sources in the off-pulse data at the location of the pulsar, and demonstrate that they are unlikely to be responsible for the same.

4.1. Positional Coincidence of an Unrelated Source

To determine the probability of finding an unrelated source coinciding with the pulsar we used the VLA FIRST catalog (Becker et al. 1985) to determine the following relationship between source counts (N) and flux density (S):

$$\log N = 2.2 - 0.826 \times \log S + \log(\delta S) + \log(A_{sky}), \quad (1)$$

where S is the flux at 1.4 GHz in mJy, δS is the flux bin width at 1.4 GHz in mJy, and A_{sky} is the area of sky under consideration in degree^2.

The area of the synthesized beam is ∼100 arcsec^2 at 325 MHz. The flux density for consideration in the equation is between $3 \times$ image-rms and 5%–10% of the pulsar flux, translated to 1.4 GHz (using spectral index $\gamma = 0.75$). The upper value is related to a realistic upper limit to the flux fraction in the off-pulse from the single-dish pulse profile (Gould & Lyne 1998). This yielded a probability of coincident unrelated sources of ∼1.5×10^{-3}. The probability of detecting coincident sources for both pulsars is the square of the above number and therefore highly improbable.

4.2. Error in Time Stamp

This scenario requires that approximately 1%–4% of the on-pulse data fall within the off-pulse gate. However, any monotonic drift in the clock, without recovery, would have smeared out the pulse obtained by folding the self-data; on the contrary, we see the on-pulse detected with a signal-to-noise ratio of 50–100 (Figure 1). Alternatively, the clock could have maintained an accurate long-term average but with large excursions in the values of the individual time stamps, i.e., excursions of the order of 1–2 s (half the pulsar period) for an output data rate of one visibility per 0.131 s or 0.262 s. This
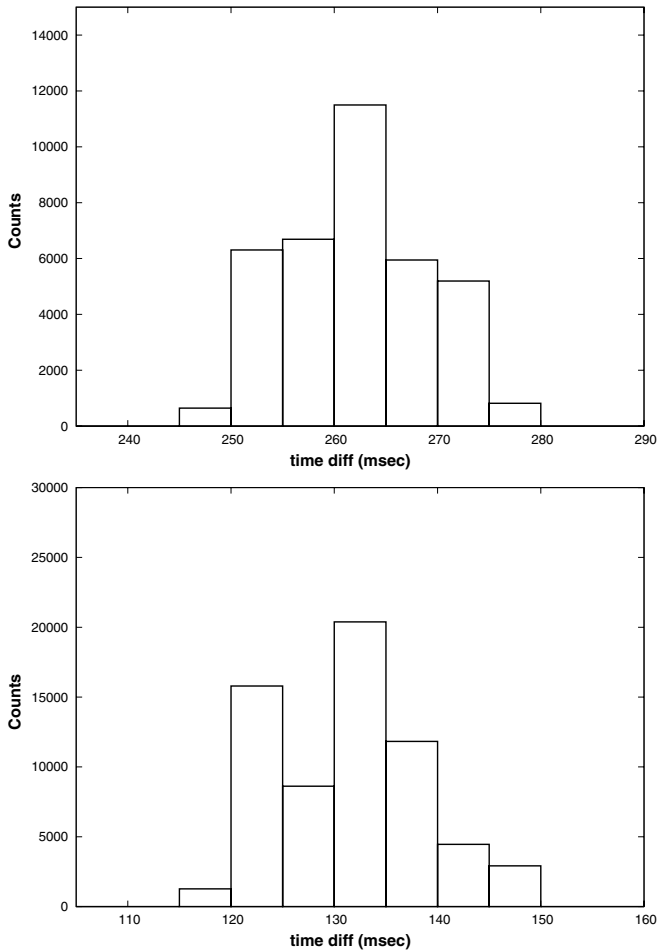
Figure 6. Auto-correlation profile for front-end terminated GMRT noise data. The scatter plot is for each baseline-channel-scan while the black line is the median profile from the scatter. The non-zero value even at large lags is indicative of non-stationary noise signal and system gain variation.

leakage would only redistribute the flux density along the time axis without causing any change in the measured flux density. Observers using the pulsar mode would not have detected such an effect because they are only sensitive to the relative flux in excess of the base level.

We tested this possibility by estimating the temporal correlation in the 0.131 s data series. Assuming that the off-pulse was entirely due to the leaking of the signal from the on-pulse bin to the off-pulse bins we estimated the required leakage for a spurious detection of the observed level. There was no way of introducing a narrow, clean pulse into the GMRT receiver system to directly measure such a leakage. So, we investigated the consequence of such a correlation on the noise data.

First, we ran simulations to estimate the auto-correlation function for noise in the presence of leakage sufficient to generate the observed off-pulse, i.e., we generated a noise series and smeared each data point into subsequent data points according to a particular time profile—e.g., constant leakage into the next 13 bins; or linearly decreasing leakage into the next 13 bins. The value 13 is related to the period of the two pulsars which covered 14 time bins.

We then recorded 6×10 minute scans of noise data (0.131 s integration) but with Front-end termination which sealed the telescope at the antenna feeds. This ensured that no temporally continuous external source (cosmic sources and RFI), which would be correlated across the entire observing session, was present in the noise data.

The auto-correlation for each baseline-channel (435×120) data was separately calculated for each scan. The median auto-correlation profile and the scatter are shown in Figure 6. The worst data are at the 0.1% level but the median is only about 0.04%. The profile does not fall to zero at large time lags, indicating non-stationarity of the noise signal. We obtained a similar behavior by introducing a time-varying mean level into the noise in our simulations. This time variation in the mean level may reflect the system gain variations as well, which would have been corrected to a greater or lesser extent by self-calibration during imaging. Therefore, the profile is a firm upper limit to the contribution of temporal leaking of signals to an off-pulse detection.

It should be noted that interferometric imaging is an excellent filter of bad data; a compact source (like the off-pulse detection) would require most of the baselines to show high temporal auto-correlation; a few bad baselines with high auto-correlation

Figure 5. Histograms of the time difference between adjacent time stamps for PSRs B0525+21 (top) and B2045−16 (bottom). The rms of the plots is 7 ms for both.

sounds somewhat contrived; if this were the case we should have expected a histogram of the time difference between adjacent data to show a large scatter. The histograms plotted in Figure 5 show a tight scatter (rms 0.007 s) around the expected mean values (0.262 s and 0.131 s).

Additionally, any artifact due to time smearing should have resulted in the shorter-period and faster-sampled B2045−16 having a higher off-pulse fraction, whereas the ratio is much higher for B0525+21.

4.3. Leakage of the Signal along the Time Series

This scenario requires temporal correlation between data separated by at least half the pulsar period. The basic sampling interval of the GMRT correlator is 31.25 ns. A cross-spectrum is output every $16\,\mu s$ by Fourier transforming 512 such samples. The data output every $16\,\mu s$ should be independent from all other such data in the time series. Eight thousand and one hundred eighty-eight (or 16,376) such independent samples are averaged to obtain the short-term acquisition (STA) data output at 0.131 s (or 0.262 s). Given the independence at the $16\,\mu s$ level it is difficult to envisage correlation between one STA and the next, even more so across 6–10 STAs (half the pulsar period). Nevertheless this was a possibility. Observers using the standard interferometric mode of the GMRT would not be affected as none of their targets vary on sub-second timescales, and their integration time is rarely less than 2 s (more typically 17 s). The
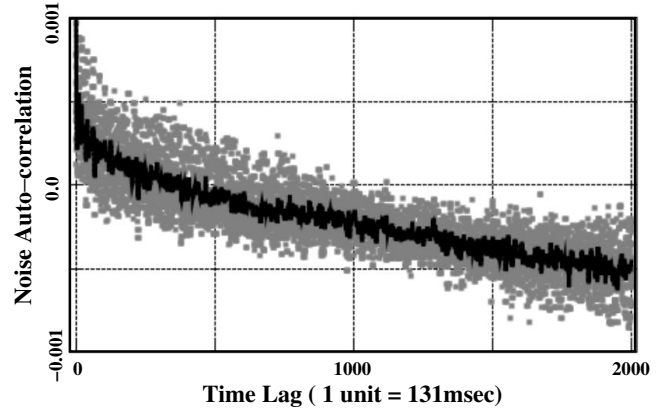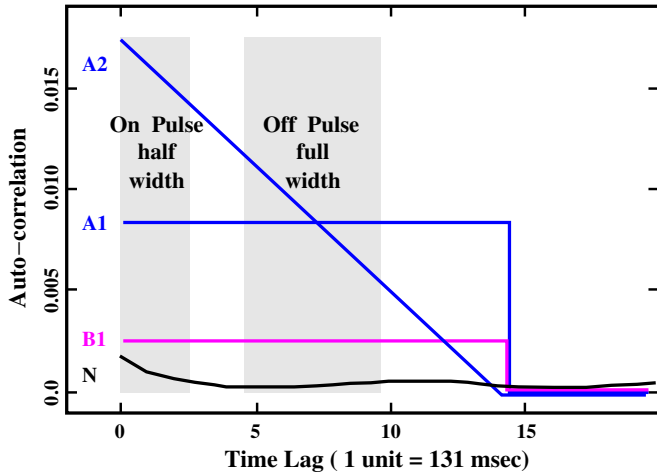
Figure 7. Expanded view of the short-lag regions of the auto-correlation profile plotted in Figure 6. The plots A1, A2 (PSR B0525+21), and B1 (PSR B2045–16) are the required (simulated) noise auto-correlation for a spurious off-pulse detection due to temporal leaking of the pulse into subsequent bins. The bottom curve (N) is the observed noise auto-correlation profile (from Figure 6).

(A color version of this figure is available in the online journal.)

would only result in noisy ripples across the image and not a localized source. Therefore, the median line is a more accurate measure of the leakage for our study than the extreme points in the scatter.

We note that non-stationarity and gain fluctuation only occur at the 0.05% level in the GMRT and would not have a discernible effect for most imaging exercises.

Figure 7 shows a magnified representation of the relevant part of the noise auto-correlation plot. A1 and A2 (both PSR B0525+21) and B1 (PSR B2045–16) indicate the required noise auto-correlation if the detected off-pulse were due to the leaking of the signal from the on-pulse bin. The analysis recipe for PSR B0525+21 (with similar arguments for PSR B2045–16) is as follows.

1. The pulsar period includes 14 time bins, each of 0.262 s. The on- and off-pulse fluxes measured over five time bins are 80.2 and 3.9 mJy, respectively. Higher time resolution observations (Gould & Lyne 1998) show that the main-pulse is narrower than one of our bins.

2. A leakage of 0.9% of the pulse flux from the first bin into each of the next 13 bins will explain the observed off-pulse. This corresponds to an auto-correlation level of 0.0087. The auto-correlation profile calculated for GMRT noise (the lowest curve "N" in Figure 7) is smaller than the required amount by a factor of at least 20.

3. A leakage reducing with temporal distance is more likely. A linearly reducing leakage (curve A2) requires a similar average auto-correlation in the off-pulse region and a higher correlation at short lags.

4. We conclude that temporal leaking of the signal is incapable of explaining the detected level of off-pulse emission.

The curve B2 represents the corresponding model for PSR B2045–16: off-pulse flux 4.3 mJy; on-pulse flux 305.2 mJy; required constant leakage 0.43%; required correlation in the off-pulse region 0.003; discrepancy is a factor of ∼6.

Additionally, the argument against time smearing (Section 4.2, second paragraph) is also valid against the leaking of the signal along the time series.

5. DISCUSSION

5.1. Previous Searches for Off-pulse Emission, Including PWNe

A literature survey yielded many reports of searches for "continuous emission in the direction of pulsars" (Table 3). Here, we shall discuss only those in which gating techniques were applied to target off-pulse emission, which could have been either from the pulsar itself or from PWNe.

Perry & Lyne (1985) reported off-pulse emission from four pulsars (PSRs B1541+09, B1604–00, B1929+10, and B2016+28) using a gated two-element interferometer at 408 MHz. Subsequent studies showed that two of these pulsars, B1541+09 and B1229+10, were aligned rotators, undermining the claim of off-pulse origin (Hankins et al. 1993; Rathnasree & Rankin 1995). The off-pulse emission in the other two pulsars, B1604-00 and B2016+28, were later identified with unrelated background sources (Strom & Van Someren Greve 1990; Hankins et al. 1993).

Bartel et al. (1985) reported a non-detection from PSR B0329+54 using gated VLBI interferometry at 2.3 GHz. Strom & Van Someren Greve (1990) reported non-detections in 43 pulsars using the WSRT in gated mode at 327 and 609 MHz. Stappers et al. (1999) reported non-detection in four pulsars using ATCA in the gated interferometric mode at 1.3 and 2.2 GHz.

Gaensler et al. (2000) searched for unpulsed emission from 27 energetic and/or high velocity pulsars using gating interferometry with the Very Large Array (VLA) and ATCA at 1.4 GHz and found emission in two cases. However, they could not conclusively determine whether these detections corresponded to PWNe or the pulsar magnetosphere; they even suggested that the detections could be spurious and a result of improper online gating. These detections were at the level of 2σ (PSR B1634−45) and 13σ (PSR B1706−16).

There have been detections of several radio pulsars with associated plerionic bow shock nebula: B1951+32 (Hester & Kulkarni 1988), B1757–24 (Frail & Kulkarni 1991), B1853+01 (Frail et al. 1996), and B1643–43 (Giacani et al. 2001). All of these are highly energetic pulsars associated with SNR (Chatterjee & Cordes 2002). Gaensler et al. (1998) reported the detection of off-pulse emission from PSR B0906–49, which appears to be a PWN generated by a slow-moving pulsar in the dense ISM.

5.2. Our Detections in the Context of Previous Efforts

We discuss here the unsuccessful search for off-pulse emission in PSR B0525+21 by Weiler et al. (1974) and Perry & Lyne (1985). Weiler et al. (1974) were looking for extended emission around the pulsar without employing any kind of gating. They had a synthesized beam size of $47'' \times 133''$ with a noise rms of 2.5 mJy beam^{-1}. It is apparent that their setup was inadequate for the present level of detection. Perry & Lyne (1985) employed a two-element interferometer with hardware gating at 408 MHz for their studies but could neither image the fields and nor correct for sensitivity variations. They listed considerable emission in the off-pulse bin for B0525+21 (in fact, greater than for B1929+10 and B2016+28, which were claimed to be positive detections) but the noise was also very high precluding a positive detection.

The major advantages of our effort were as follows.

1. *Low frequency of observation.* The steep spectrum pulsar is likely to dominate over emission from any associated nebula with flatter spectrum.

Table 3
Literature Survey for Off-pulse Studies

Non Detections/ Subsequent SNR	Detections Later Refuted	Tentative Detection	PWNe Detection
1. Schönhardt 1973, 1974	1. Gopal-Krishna 1978	1. Gaensler et al. 2000 (*G*)	1. Frail & Kulkarni 1991
2. Weiler et al. 1974	2. Glushak et al. 1981		2. Frail et al. 1996
3. Cohen et al. 1983	3. Perry & Lyne 1985 (*G*)		3. Gaensler et al. 1998
4. Bartel et al. 1985 (*G*)			4. Giacani et al. 2001
5. Strom & Van Someren Greve 1990 (*G*)			
6. Hankins et al. 1993 (*G*)			
7. Frail & Scharringhausen 1997			
8. Stappers et al. 1999 (*G*)			

Notes. There have been no unambiguous detection of off-pulse emission not associated with PWNe. The gated interferometry studies in Table 3 have been indicated with *G*.

2. *A multi-element interferometer.* The GMRT is currently the most sensitive low-frequency instrument. The ability to correct gain variations, filter bad data using imaging residuals and RFI excision tools (Athreya 2009) allowed us to make sufficiently deep images.

3. *Off-line gating of data.* This allowed secure separation of the off- and on-pulse sections.

5.3. PWN Emission

The confinement of the relativistic wind from pulsars generates PWNe which are luminous across the electromagnetic spectrum in synchrotron, inverse Compton, and optical line emission from the shocked regions. All known PWNe seen around radio pulsars have spin-down luminosities $\dot{E} \gtrsim 10^{34}$ erg s^{-1}. They all appear to be young and, with the exception of PSR B0906–49 (Gaensler et al. 1998), are associated with SNRs. Two classes of PWNe can be formed in the absence of associated SNRs: one, where the pulsar wind is confined by the density of the ISM— known as static PWN; and the other, where the wind is confined by the ram pressure of motion of the pulsar through the ISM— called bow shock nebula. Our two target pulsars, B0525+21 and B2045–16, are not associated with SNRs. So, we explored the possibility that the detected off-pulse emission was due to a PWN.

The efficiency factor ϵ_R is defined as the ratio of the radio bolometric luminosity (L_R) of a PWN to the spin-down energy ($\dot{E}$) of the pulsar $L_R = \epsilon_R \dot{E}$. If we assume a typical PWN spectral index of $\gamma \sim 0.3$, its radio luminosity between 10^7 Hz and 10^{11} Hz is given by $L_R = 3.06 \times 10^{28} d_{\rm kpc}^2 S_{\rm mJy}$ erg s^{-1}, where $d_{\rm kpc}$ is the distance to the PWN in kpc and $S_{\rm mJy}$ is the integrated flux of PWN at 325 MHz in mJy. Using the measured flux density (Table 2), source distance, and spin-down energies (Table 1), we calculate efficiency factors of 2×10^{-2} for B0525+21 and 2×10^{-3} for B2045–16. These ϵ_R values are 1–2 orders of magnitude higher than those of previously known PWNe (typical $\epsilon_R \sim 10^{-4}$; see Frail & Scharringhausen 1997; Gaensler et al. 2000 for a discussion).

Static PWN. The relativistic particles and Poynting flux emanating from the pulsar, at rest relative to the ISM, will drive through the ambient medium a shock of radius R_s given by (Arons 1983)

$$R_s = \left(\frac{\dot{E}}{4\pi\rho_o} \right)^{1/5} t^{3/5}. \qquad (2)$$

The velocity of the shock front is given by

$$\dot{R}_s = \frac{3}{5} \left(\frac{\dot{E}}{4\pi\rho_o t^2} \right)^{1/5} = 3.3 \left(\frac{\dot{E}_{31}}{t_6^2 n_{0.01}} \right)^{1/5} {\rm km\,s^{-1}}. \qquad (3)$$

Here, $\rho_o = m_H n$, where m_H is the proton mass and n is the particle density of the ISM. Using Equation (2) the required particle density for a PWN is

$$n = 5.35 \times 10^{11} \left(\frac{\dot{E}_{31} t_6^3}{R_{0.01}^5} \right) {\rm cm^{-3}}, \qquad (4)$$

where $\dot{E}_{31}$ is the spin-down power in units of 10^{31} erg s^{-1}, t_6 is the age in units of 10^6 yr, $R_{0.01}$ is the radius of PWN in units of 0.01 pc, and $n_{0.01}$ is the ISM density in units of 0.01 cm^{-3}. In the present exercise, we assume that the PWNe in our targets are smaller than one synthesized beam width since the off-pulse emission is unresolved in both pulsars. Using Equation (4) and values in Tables 1 and 2, we determined the ISM density required to drive a PWN to be $\sim 3 \times 10^9$ cm^{-3} for B0525+21 and $\sim 10^{12}$ cm^{-3} for B2045–16. The required particle densities are much higher than typical ISM densities of ~ 0.03 cm^{-3}, suggesting that these pulsars are too weak and old to power a static PWN through the ISM. Since our estimates of the sizes of the nebulae are upper limits the particle density estimates are lower limits.

Bow shock PWN. This requires that the shock velocity ($\dot{R}_s$) be much smaller than the pulsar transverse velocity ($V_{\rm PSR}$). The typical ISM density of 0.03 cm^{-3} in Equation (3) yields $\dot{R}_s \sim 2.8$ km s^{-1} for B0525+21 and ~ 2.5 km s^{-1} for B2045–16, which are indeed much smaller than the $V_{\rm PSR}$ listed in Table 1. The radius of the shock is given by (Frail & Scharringhausen 1997)

$$R_{\rm BS} = \left(\frac{\dot{E}}{4\pi c \rho_o V_{\rm PSR}^2} \right)^{1/2}. \qquad (5)$$

From Equation (5) the particle density required to sustain a bow shock PWN is

$$n = 1.67 \times 10^{-4} \left(\frac{\dot{E}_{31}}{R_{0.01}^2 V_{100}^2} \right) {\rm cm^{-3}}, \qquad (6)$$

where $\dot{E}_{31}$ is the spin-down power in units of 10^{31} erg s^{-1}, $R_{0.01}$ is the radius of the PWN in units of 0.01 pc, and V_{100} is the

velocity of the pulsar through the ISM in units of 100 km s^{-1}. This requires an ISM density of $\sim 5 \times 10^{-6} \text{ cm}^{-3}$ for B0525+21 and $\sim 8 \times 10^{-6} \text{ cm}^{-3}$ for B2045–16. These values are 3–4 orders of magnitude lower than the typical ISM density. This implies that the pulsars are too weak to drive a bow shock nebula of the size corresponding to the telescope resolution. However, a bow shock interpretation can be salvaged if the nebulae are ~ 2 orders of magnitude smaller.

In summary, identifying the off-pulse emission detected here with PWNe results in unrealistic values of the ISM particle density. This is not surprising because we selected as our targets middle-aged pulsars, a category which has hitherto not been known to be associated with PWNe.

5.4. Emission from the Magnetosphere

Numerous published studies provide estimates of α and β for the pulsars studied here. Some use an empirical/geometrical (E/G) approach to establish α and β (Lyne & Manchester 1988; Rankin 1993; see Everett & Weisberg 2001 for a discussion on the E/G approach). One can also obtain α and β values by fitting the RVM to the PPA traverse (Mitra & Li 2004), but these fits yield highly correlated estimates of the two angles. This issue has been discussed in depth by Everett & Weisberg (2001) and Mitra & Li (2004).

Everett & Weisberg (2001) list six different studies of PSR B0525+21 with α ranging from $116°$ to $159°$.[5] Mitra & Li (2004) estimated $\alpha \sim 127°$–$144°$ for PSR B2045–16. Both RVM fit and the E/G approach were used to obtain the above estimates of α. These studies provide good evidence that our targets, B0525+21 and B2045–16, are not aligned rotators and therefore any off-pulse emission must arise far from the magnetic pole.

The pulse profiles of both these pulsars show sharp rising and falling edges. PSR B0525+21 is an example of a classical double (D) profile, whereas PSR B2045–16 is classified as a triple (Rankin 1993). The main-pulse width for these pulsars span about 5% of the period, and there are no obvious emission components visible outside the main-pulse. Based on the pulse widths and the estimates of α and β, Mitra & Li (2004) concluded that the radio emission arises at a distance of 1%–2% of the light cylinder. Hence, the radio on-pulse emission of PSR B0525+21 and B204516 are classical examples of emission from open dipolar field lines. The remaining 95% of the period, i.e., the off-pulse region, were hitherto thought to be radio-quiet zones of the pulsar magnetosphere (Goldreich & Julian 1969; Ruderman & Sutherland 1975).

Our off-pulse longitude corresponds to $80°$–$208°$ (from the peak of the main-pulse) for B0525+21 and $101°$–$229°$ for B2045–16. In a few cases, PPC emissions have been detected about $60°$ from the main-pulse, posing questions regarding their origin (Mitra & Rankin 2011). Our detections are even further away from the main-pulse. It remains to be seen if these off-pulse detections are an extreme example of PPC or if it represents unpulsed emission from throughout the pulse period.

It is to be noted that the opening angle of dipolar field lines scales as the square of the emission height. If radio emission from pulsars originate from higher up the light cylinder ($\gg$ 1%–2% of the light cylinder), the polar emission could span

a larger longitudinal range. This implies that radio emissions at larger distances from the neutron star surface are potential sites of PPC or off-pulse emission in pulsars. Alternatively, if the emission arises close to the neutron star surface, the emitting region will need to encroach upon the closed field lines of the neutron star. Thus, the existence of magnetospheric off-pulse emission should prove to be an important input for pulsar electrodynamic models which try to establish the relation between magnetospheric currents and coherent pulsar radio emission (Spitkovsky 2006).

6. CONCLUSION

We report GMRT observations at 325 MHz which detected off-pulse emission from two long-period pulsars which have low spin-down rates and are not associated with SNRs. We have adduced evidence that the signals are neither artifacts of the observing procedure, nor unrelated background sources which happen to be coincident with the pulsar. We have argued that explaining these detections as PWN requires ISM particle densities which differ from typical measured values by several orders of magnitude. Robust estimates of the geometrical parameters of these two pulsars argue against them being aligned rotators. This leaves the possibility of emission from the magnetosphere. If the off-pulse emission arises from a much higher height than the on-pulse then it could arise from open field lines at the edge of the light cylinder. On the other hand, if the off-pulse emission is from the same height as the on-pulse emission then it must be associated with closed field lines. Further studies at multiple frequencies, in polarization and higher resolution, are needed to establish the nature of this emission which can impose valuable constraints on the pulsar emission mechanism models.

REFERENCES

Arons, J. 1983, Nature, 302, 301
Athreya, R. 2009, ApJ, 696, 885
Baars, J. W. M., Genzel, R., Pauliny-Toth, I. I. K., & Witzel, A. 1977, A&A, 61, 99
Backus, I., Mitra, D., & Rankin, J. M. 2010, MNRAS, 404, 30
Bartel, N., Ratner, M. I., Shapiro, I. I., Cappallo, R. J., Rogers, A. E. E., & Whitney, A. R. 1985, AJ, 90, 318
Becker, R. H., White, R. L., & Helfand, D. J. 1995, ApJ, 450, 559
Blandford, R. D., Ostriker, J. P., Pacini, F., & Rees, M. J. 1973, A&A, 23, 145
Chatterjee, S., & Cordes, J. M. 2002, ApJ, 575, 407
Cohen, N. L., Cotton, W. D., Geldzahler, B. J., & Marcaide, J. M. 1983, ApJ, 264, 273
Everett, J. E., & Weisberg, J. M. 2001, ApJ, 553, 341
Frail, D. A., Giacani, E. B., Goss, W. M., & Dubner, G. 1996, ApJ, 464, 165
Frail, D. A., & Kulkarni, S. R. 1991, Nature, 352, 785
Frail, D. A., & Scharringhausen, B. R. 1997, ApJ, 480, 364
Gaensler, B. M., Stappers, B. W., Frail, D. A., & Johnston, S. 1998, ApJ, 499, 69
Gaensler, B. M., Stappers, B. W., Frail, D. A., Moffett, D. A., Johnston, S., & Chatterjee, S. 2000, MNRAS, 318, 58
Giacani, E. B., Frail, D. A., Goss, W. M., & Vieytes, M. 2001, AJ, 121, 3133
Glushak, A. P., Pynzar, A. V., & Udaltsov, V. A. 1981, SvA, 25, 182

---

[5] Following Everett & Weisberg (2001), α values should span $0°$–$180°$ (and not $0°$–$90°$) for a consistent definition of the pulsar rotation axis. Everett & Weisberg provide a compilation of published α and β values corrected for this convention.

Goldreich, P., & Julian, W. H. 1969, ApJ, 157, 869
Gopal-Krishna 1978, MNRAS, 185, 521
Gould, D. M., & Lyne, A. G. 1998, MNRAS, 301, 235
Hankins, T. H., Moffett, D. A., Novikov, A., & Popov, M. 1993, ApJ, 417, 735
Hankins, T. H., & Rickett, B. J. 1975, MComP, 14, 55
Hester, J. J., & Kulkarni, S. R. 1988, ApJ, 331, L121
Hobbs, G., Lyne, A. G., Kramer, M., Martin, C. E., & Jordan, C. 2004, MNRAS, 353, 1311
Lorimer, D. R., Yates, J. A., Lyne, A. G., & Gould, D. M. 1995, MNRAS, 273, 411
Lyne, A. G., & Manchester, R. N. 1988, MNRAS, 234, 477
Mitra, D., & Li, X. H. 2004, A&A, 421, 215
Mitra, D., & Rankin, J. M. 2011, ApJ, in press (arXiv:1011.0556)
Perley, R. A., Lacey, C. K., Jones, D. L., Weiler, K. W., Kaiser, M. L., & Allen, R. J. 1999, BAAS, 31, 836
Perry, T. E., & Lyne, A. G. 1985, MNRAS, 212, 489
Radhakrishnan, V., & Cooke, D. J. 1969, ApL, 3, 225
Rankin, J. M. 1993, ApJ, 405, 285
Rathnasree, N., & Rankin, J. M. 1995, ApJ, 452, 814
Ruderman, M. A., & Sutherland, P. G. 1975, ApJ, 196, 51
Schönhardt, R. E. 1973, Nature Phys. Sci., 243, 62
Schönhardt, R. E. 1974, A&A, 35, 13
Spitkovsky, A. 2006, ApJ, 648, L51
Stappers, B. W., Gaensler, B. M., & Johnston, S. 1999, MNRAS, 308, 609
Stinebring, D. R., & Condon, J. J. 1990, ApJ, 352, 207
Strom, R. G., & Van Someren Greve, H. W. 1990, Ap&SS, 171, 351
Swarup, G., Ananthakrishnan, S., Kapahi, V. K., Rao, A. P., Subrahmanya, C. R., & Kulkarni, V. K. 1991, CuSc, 60, 95
Taylor, J. H., Manchester, R. N., & Lyne, A. G. 1993, ApJS, 88, 529
Weiler, K. W., Goss, W. M., & Schwarz, U. J. 1974, A&A, 35, 473